

The Contribution of Galaxies to the 3.4 μm Cosmic Infrared Background as Measured Using *WISE*

S. E. LAKE,^{1,2,3} E. L. WRIGHT,³ R. J. ASSEF,⁴ T. H. JARRETT,⁵ S. PETTY,⁶ S. A. STANFORD,^{7,8} C.-W. TSAI,^{1,2,3}

¹*National Astronomical Observatories, Chinese Academy of Sciences, Beijing, 100012, People's Republic of China*

²*CAS Key Laboratory of FAST, NAOC, Chinese Academy of Sciences, People's Republic of China*

³*Physics and Astronomy Department, University of California, Los Angeles, CA 90095-1547*

⁴*Núcleo de Astronomia de la Facultad de Ingeniería, Universidad Diego Portales, Av. Ejército 441, Santiago, Chile*

⁵*Astronomy Department University of Cape Town Private Bag X3 Rondebosch 7701 Republic of South Africa*

⁶*NorthWest Research Associates 4118 148th Ave NE Redmond, WA 98052-5164*

⁷*Institute of Geophysics and Planetary Physics, Lawrence Livermore National Laboratory, Livermore CA 94551*

⁸*Department of Physics, University of California, Davis, CA 95616*

ABSTRACT

The study of the extragalactic background light (EBL) in the optical and near infrared has received a lot of attention in the last decade, especially near a wavelength of $\lambda \approx 3.4 \mu\text{m}$, with remaining tension among different techniques for estimating the background. In this paper we present a measurement of the contribution of galaxies to the EBL at 3.4 μm that is based on the measurement of the luminosity function (LF) in Lake et al. (2018) and the mean spectral energy distribution of galaxies in Lake & Wright (2016). The mean and standard deviation of our most reliable Bayesian posterior chain gives a 3.4 μm background of $I_\nu = 9.0 \pm 0.5 \text{ kJy sr}^{-1}$ ($\nu I_\nu = 8.0 \pm 0.4 \text{ nW m}^{-2} \text{ sr}^{-1} e\text{-fold}^{-1}$), with systematic uncertainties unlikely to be greater than 2 kJy sr^{-1} . This result is higher than most previous efforts to measure the contribution of galaxies to the 3.4 μm EBL, but is consistent with the upper limits placed by blazars and the most recent direct measurements of the total 3.4 μm EBL.

Keywords: galaxies: evolution, galaxies: statistics

1. INTRODUCTION

The extragalactic background light (EBL) is another name for a fundamental component of the cosmos: the overall spectrum and density of photons in the universe. In terms of both quantity of energy and number of photons the dominant component of the EBL is the cosmic microwave background (CMB).¹ While the study of the CMB provides a wealth of information about both the universe at the time those photons were emitted and how the evolving universe has modified those photons, there is a lot to be learned from the study of the EBL frequencies that are dominated by photons emitted at different epochs. Studies of the whole of the EBL have revealed that there are, broadly speaking, four peaks in its spectral energy distribution (SED): the CMB in

the rough wavelength range 320 μm to 22 mm, a dust emission of galaxies peak from 64 to 700 μm , a stellar photospheric peak from 0.15 μm to 4 μm , and an active galactic nuclei (AGN) and stellar remnant peak in X-rays from 4 to 580 pm (see Cooray 2016).

While the energy content of the radiation field (of which the EBL is a part) has had a sub-dominant impact on the evolution of space-time, itself, since the redshift of matter-radiation equality (around $z = 3000$; Hinshaw et al. 2013), its spectrum encodes useful information about the history of star and structure formation in the universe. With the exception of high energy photons (energy roughly higher than the Lyman- α transition), once the intergalactic medium achieved full reionization the universe became transparent. The primary consequence of this is that once a photon escapes from the dense matter in a galaxy halo it has a low probability of ever scattering again, leaving it to eventually be redshifted into oblivion by cosmic expansion. This means that when we sample the small fraction of the EBL that reaches our detectors, we are sampling an integrated record of all the light the universe has emitted.

Corresponding author: S. E. Lake
lake@nao.cas.cn

¹ In some usages the EBL and CMB are regarded as distinct, here we follow the usage in Cooray (2016) that agrees with the plain meaning of the words.

The primary challenge in directly measuring the EBL is removing the large glare of foreground sources, especially the reflected sunlight from dust in our solar system known as the zodiacal light (studies using this approach include: Gorjian et al. 2000; Wright & Reese 2000; Cambr esy et al. 2001; Wright & Johnson 2001; Matsumoto et al. 2005; Levenson et al. 2007; Tsumura et al. 2013; Sano et al. 2016). It is for that reason that two other techniques have come to the fore in the attempts to study the EBL in the optical and near-infrared. The first is to study individually detected galaxies, directly, and extrapolating to the undetected galaxies to estimate how much light galaxies have released into the EBL (for example: Fazio et al. 2004; Levenson & Wright 2008; Dom nguez et al. 2011; Helgason et al. 2012; Driver et al. 2016; Stecker et al. 2016). The challenge with this technique lies in the accuracy of the extrapolation technique used. The second is to leverage the fact that low energy photons can pair produce with very high energy photons, providing opacity to them (for example: Aharonian et al. 2006; Mazin & Raue 2007). Ideally this means that high energy gamma rays produced by blazars, typically in the TeV range of energy, are sampling the EBL directly in intergalactic space. The catch that limits the accuracy of this technique is the limit of our ability to determine the gamma ray spectrum pre-extinction, including the production mechanisms and location (see, for example, Essey & Kusenko 2010).

There is controversy in this field in the measurement of the background in the range of 1–4 μm where direct measures are higher than the upper limits from gamma ray blazars by about a factor of 2, and the lower limits from extrapolating number counts are not definitive. With the goal of providing more information relevant to the discussion around 3.4 μm , this work is based on the extrapolation technique. Rather than extrapolating the flux histogram, as was done in Fazio et al. (2004); Levenson & Wright (2008); Driver et al. (2016), this work uses an approach based on extrapolating the galaxy luminosity function (LF), as was done in Dom nguez et al. (2011); Helgason et al. (2012); Stecker et al. (2016). In contrast to previous LF based extrapolation measurements, where they extrapolated extant LFs from the literature, this work is based on a measurement of the LF from scratch that leveraged six public spectroscopic redshift databases of diverse depth and breadth with multiple public photometry databases (especially ALLWISE) to construct multiple LFs. Translating an LF measurement into an EBL estimate requires something equivalent to the mean SED of galaxies, too (previous works used LFs at multiple wavelengths to work around measuring this directly). To measure this quantity we used

only the zCOSMOS data set because of its depth and exceptional variety of photometric information. Along the way, decisions about what data to use were all optimized for measuring the contribution of galaxies to the EBL at 3.4 μm . The reliance on spectroscopic redshifts reduces the exposure to systematic uncertainties inherent in photometric redshift surveys, and the measurement of a new LF from scratch permits us to feed forward all of the information about the significant correlations among estimated LF parameters into the background estimates.

The structure of this paper is as follows: Section 2 covers the equations that relate the LF and mean SED of galaxies to the source flux histogram and integrated background, Section 3 contains a short summary of the results from previous paper used to measure the background and its uncertainty, Section 4 presents estimates of the 3.4 μm background and flux histograms at various wavelengths, and Section 5 discusses how our results compare to previous estimates in the literature.

The cosmology used in this paper is based on the WMAP 9 year ΛCDM cosmology (Hinshaw et al. 2013)², with flatness imposed, yielding: $\Omega_M = 0.2793$, $\Omega_\Lambda = 1 - \Omega_M$, redshift of recombination $z_{\text{recom}} = 1088.16$, and $H_0 = 70 \text{ km sec}^{-1} \text{ Mpc}^{-1}$. All magnitudes will be in the AB magnitude system, unless otherwise specified. When computing bandpass solar luminosities we utilized the 2000 ASTM Standard Extraterrestrial Spectrum Reference E-490-00³. For our standard bandpass, W1 at $z = 0.38$, we calculate the absolute magnitude of the sun to be $M_{2.4 \mu\text{m} \odot} = 5.337 \text{ AB mag}$, $L_{2.4 \mu\text{m} \odot} = 3.344 \times 10^{-8} \text{ Jy Mpc}^2$ from that spectrum.

2. THEORETICAL TOOLS

The basis of the calculations in this work is a mathematical object called the spectro-luminosity functional, denoted $\Psi[L_\nu](\nu)$, that is related to galaxy SEDs in the same way that the ordinary LF is related to regular luminosity. In words it is the mean number of galaxies per unit comoving volume per unit function space volume. Lake et al. (2017) contains a fuller treatment of Ψ . One property of Ψ is that the comoving spectral luminosity density ρ_ν (L_ν per unit comoving volume, related to the spectral emission coefficient of radiative transfer, j_ν , by a factor of 4π), is the first moment of it:

$$\rho_\nu = \int [\mathcal{D}L_\nu] L_\nu \Psi[L_\nu](z). \quad (1)$$

² http://lambda.gsfc.nasa.gov/product/map/dr5/params/lcdm_wmap9.cfm

³ <http://rredc.nrel.gov/solar/spectra/am0/>

Splitting $\Psi[L_\nu](z)$ into the traditional luminosity function, $\Phi(L_f, z)$, and the likelihood of a galaxy having an SED given that a normalization luminosity is fixed (the normalized SED is $\ell_\nu(\nu) \equiv L_\nu(\nu)/L_f$, with $f = c/[2.4 \mu\text{m}]$, here) gives:

$$\begin{aligned} \rho_\nu &= \int dL_f \int [\mathcal{D}\ell_\nu] \ell_\nu \mathcal{L}_{\text{SED}}[\ell_\nu](\cdot|L_f, z) L_f \Phi(L_f, z) \\ &= \int dL_f \mu_\nu(\nu[1+z], L_f, z) L_f \Phi(L_f, z), \end{aligned} \quad (2)$$

where $\mathcal{L}_{\text{SED}}[\ell_\nu](\cdot|L_f, z)$ is the likelihood that a galaxy at redshift z with spectral luminosity L_f at $f = c/[2.4 \mu\text{m}]$ will have the normalized SED given by ℓ_ν . The dot and vertical pipe character, ‘|’, are there to emphasize that L_f and z are treated as non-random variables for \mathcal{L}_{SED} , in the same way the notation is used for conditional probabilities. This is relevant because it affects what units \mathcal{L}_{SED} has; it is a density with respect to the random variables, and not the non-random ones. The second line of Equation 2 is an application of the definition of the mean normalized SED, $\mu_\nu \equiv \langle \ell_\nu \rangle$.

The transition from spectral luminosity density to the background is achieved by treating each infinitesimal comoving volume element, dV_c , as a galaxy with SED $L_\nu = \rho_\nu dV_c$ that subtends a solid angle $d\Omega$. The relationship between observed flux surface brightness, $\frac{dF_\nu}{d\Omega} \equiv I_\nu$, which is the physical quantity that defines the EBL, then follows from the definition of luminosity distance, $D_L(z)$:

$$\begin{aligned} F_\nu(\nu_{\text{obs}}) d\nu_{\text{obs}} &= \frac{L_\nu(\nu_{\text{rest}}) d\nu_{\text{rest}}}{4\pi D_L^2(z)} \Rightarrow \\ \frac{dI_\nu(\nu)}{dz} &= \frac{\rho_\nu([1+z]\nu, z)}{4\pi[1+z]D_{cT}^2(z)} \left(\frac{dV_c}{dz} \right) \frac{1}{\Omega_{\text{sky}}} \\ &= \frac{\rho_\nu([1+z]\nu, z)}{\Omega_{\text{sky}}[1+z]} \left(\frac{dD_c}{dz} \right), \end{aligned} \quad (3)$$

where D_c is the radial comoving distance at redshift z .

In the absence of emission, cosmological dimming for any surface brightness has four factors of $1+z$ in it, so $I_\nu(\nu, 0) d\nu_{\text{obs}} = (1+z)^{-4} I_\nu(\nu, z) d\nu_{\text{rest}}$. It is useful to

$$\begin{aligned} \frac{d^2 N}{dF_\nu d\Omega} &= \frac{1}{\Omega_{\text{sky}}} \int dz \int dL_f \delta \left(F_\nu - \frac{L_f \mu_\nu(\nu[1+z], L_f, z)}{4\pi[1+z]D_{cT}^2(z)} \right) \frac{dV_c}{dz} \Phi(L_f, z) \\ &= \frac{16\pi^2}{\Omega_{\text{sky}}} \int dz \frac{dD_c}{dz} \left(\frac{[1+z]D_{cT}^4(z)}{\mu_\nu(\nu[1+z], L_f, z)} \right) \Phi \left(\frac{F_\nu 4\pi[1+z]D_{cT}^2(z)}{\mu_\nu(\nu[1+z], L_f, z)}, z \right), \end{aligned} \quad (7)$$

where $D_{cT}(z)$ is the comoving distance transverse to the line of sight (also called D_M for ‘proper motion’ distance).

use Equation 3 to add the effect of emission to this expression, producing a relation between the EBL at one redshift and the EBL at another. This allows for the calculation of an evolving EBL, and the ability to combine different models that are valid at different redshifts in a straightforward way. That combination is:

$$\begin{aligned} I_\nu(\nu, z) &= \frac{[1+z]^3}{\Omega_{\text{sky}}} \int_z^{z_f} \rho_\nu(\nu[1+z'], z') c \frac{dt_L}{dz'} dz' \\ &\quad + \left(\frac{1+z}{1+z_f} \right)^3 I_\nu(\nu, z_f), \end{aligned} \quad (4)$$

where $c \frac{dt_L}{dz} = \frac{1}{1+z} \frac{dD_c}{dz}$, and ρ_ν is defined in Equation 2. It should be reiterated that the frequency, ν , is as measured at $z = 0$, making it a comoving/coordinate frequency, and $[1+z]\nu$ is the rest frame (physical) frequency at z .

Combining Equations 2 and 3 gives the contribution to the background per unit luminosity per unit redshift:

$$\frac{d^2 I_\nu}{dz dL_\nu} = \frac{\mu_\nu([1+z]\nu, L_f, z)}{\Omega_{\text{sky}}[1+z]} \left(\frac{dD_c}{dz} \right) L_f \Phi(L_f, z). \quad (5)$$

Note that the more familiar K -correction can be written in terms of μ_ν as $K = -2.5 \log_{10}([1+z] \cdot \mu_\nu)$. The quantity in Equation 5 is useful enough to assign it a symbol of its own, since it is the density of contribution to the background, $\mathcal{B}_\nu(\nu) \equiv \frac{d^2 I_\nu}{dz dL}$.

Equation 5 can be integrated directly to calculate the predicted background at any frequency, but since the EBL can also be calculated from the integral of the flux times the density of sources per unit flux per unit solid angle,

$$I_\nu = \int_0^\infty dF_\nu F_\nu \frac{d^2 N}{dF_\nu d\Omega}, \quad (6)$$

it is worthwhile to derive an expression for the source counts in order to provide a more detailed check on the LF model in comparison to data not used in the measurement. The number of galaxies per unit observed flux per unit solid angle on the sky is given by:

3. SUMMARY OF RESULTS USED

As Equation 5 shows, the two necessary quantities for calculating the EBL are the mean SED of galaxies and

the LF. For the mean SED, this work uses the overall mean from Lake & Wright (2016) that was constructed from fitting templates from Assef et al. (2010) to targets in the redshift range $z \in (0.05, 1]$ (median 0.57) from the zCOSMOS survey described in Lilly et al. (2009) and Knobel et al. (2012). The resulting mean SED is shown in Figure 1. The plot also contains the $1\text{-}\sigma$ band of SED variety around the mean SED because where the width of that band compared to the position of the mean SED becomes too great determines where the Gaussian approximation of \mathcal{L}_{SED} begins to break down. The vertical lines are guides to where particular parts of the mean SED contribute to the $3.4\ \mu\text{m}$ EBL.

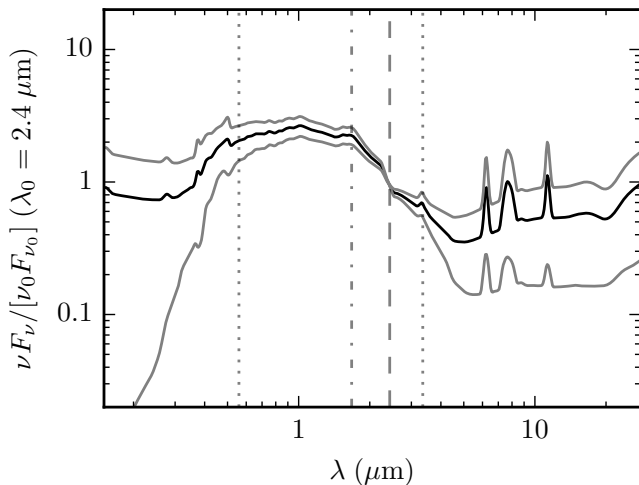


Figure 1. Mean Galaxy SED with Variety Band

The mean SED of galaxies as approximated using fits to the templates in Assef et al. (2010) done in Lake & Wright (2016). The grey lines show the band of $1\text{-}\sigma$ in SED variety, and the accuracy of the Gaussian approximation is limited to regions where that band is sufficiently narrow compared to the mean SED. The vertical lines are guides to the parts of the mean SED that galaxies at particular redshifts contribute to the $3.4\ \mu\text{m}$ background. The vertical dashed line shows the effective rest frame wavelength of W1 for galaxies at $z = 0.38$ ($\lambda \approx 2.4\ \mu\text{m}$), the vertical dotted line shows the same for galaxies at $z = 0$ and $z = 5$, and the vertical dash-dotted line is for galaxies at $z = 1$.

For the LF this work uses the set of Markov Chain Monte Carlo (MCMC) chains that sample the posterior probability of LF parameters from Lake et al. (2018) and available under digital object identifier (DOI) 10.6084/m9.figshare.4109625. The measurement that produced the chains is based on a combination of several spectroscopic redshift data sets with public photometric databases, especially the AllWISE data release. The LF that the chains have parameters for is a

Schechter LF:

$$\Phi(L_f, z) = \frac{\phi_*(z)}{L_*(z)} \left(\frac{L_f}{L_*(z)} \right)^\alpha e^{-L_f/L_*(z)}. \quad (8)$$

The evolution models for ϕ_* and L_* are similar to the commonly used Lin et al. (1999), modified to use look-back time, $t_L(z)$, instead of redshift. The model for L_* also sets $L_*(t_0) = 0$ at some lookback time t_0 when galaxies first lit up, forcing L_* to peak at some finite redshift. The exact parameterizations are:

$$\begin{aligned} \phi_*(t_L) &= \phi_0 e^{-R_\phi t_L}, \quad \text{and} \quad (9) \\ L_*(t_L) &= L_0 e^{-R_L t_L} \left(1 - \frac{t_L}{t_0} \right)^{n_0}, \quad (10) \end{aligned}$$

where ϕ_0 , R_ϕ , L_0 , R_L , α , n_0 , and t_0 are all constants. The only constant not, in some way, measured is t_0 which is set to the lookback time of recombination, equivalent to the redshift $z_{\text{recomb}} = 1088.16$ according to the WMAP 9 year ΛCDM parameters matrix of Hinshaw et al. (2013)⁴ (giving $t_0 = 0.9828 t_H = 13.73$ Gyr). Using $z_{\text{reion}} = 10.6$ gives similar results, despite the fact that galaxies must have been producing light before then, so the results are not very sensitive to the details of t_0 , as long as $L_*(t_0)$ is small enough to force a turnover in $L_*(t)$. Full details of how to extract these parameters from the contents of the chain files are given in Lake et al. (2018).

Lake et al. (2018) has 12 different MCMC posterior chains: one for each of the six surveys, and six that combine the data in different ways (primarily to work around an issue with bright sources in the low redshift data). Producing this many different analyses gives a good handle on any systematic issues. Of the 12 chains, the two combined data ones that use high redshift data with a prior on α are preferred because the data from many redshifts is needed to constrain the evolution rate parameters, to which the background is very sensitive. These samples are denoted ‘‘High z Prior’’ and ‘‘High z Trim Prior’’. Of the two, the former is preferred because it has a much larger sample size, though the latter is less sensitive to the details of the spectro-luminosity model that, effectively, determined the completeness model.

For every set of parameters in the LF chains two backgrounds are calculated: the background from sources with $z \leq 1$, and from sources with $z \leq 5$. The first redshift limit is set to match the upper limit on the data used to measure the LFs, and so marks the lower edge of model validity. The upper limit at $z = 5$ is set to capture as much of the background predicted by the model

⁴ https://lambda.gsfc.nasa.gov/product/map/current/params/lcdm_wmap9.cfm

as possible without relying on the parts of the mean SED where the size of the SED covariance makes the Gaussian approximation of \mathcal{L}_{SED} invalid.

4. BACKGROUNDS AND NUMBER COUNTS

The primary result from [Lake et al. \(2018\)](#) is a collection of posterior MCMC chains for evolving luminosity function parameters. When combined with the mean SEDs from [Lake & Wright \(2016\)](#), it is possible to calculate a couple of different interesting quantities. First, we combine each element from the chains to calculate a background observable now, giving MCMC posterior chains for the EBL. Second, we use the mean LF parameters from the ‘High z Prior’ chain to calculate predicted histograms of galaxies, and compare them to observed histograms of all sources. Third, using the same combination used to calculate the number counts, we also calculate an evolving spectral luminosity density and EBL as a function of comoving wavelength from 0.5–5 μm , quantities useful in predicting the total opacity to very high energy gamma rays.

The backgrounds that correspond to the posterior MCMC chains from [Lake et al. \(2018\)](#) are published alongside this article as a machine readable table, and under [DOI:10.6084/m9.figshare.4245443](https://doi.org/10.6084/m9.figshare.4245443). Each posterior LF chain has a corresponding file containing the backgrounds calculated for each element in the LF chain. Examples of histograms constructed using the posterior chains can be found in [Figure 2](#), and a few example lines from one of the posterior tables are in [Table 1](#). Except for the smallest data set plotted, the black lines of Panel **c**, all of the distributions are visually similar to log-normal distributions.

The symmetry of the histograms in log-space makes a description of each result as a log-normal distribution, parameterized by its geometric mean, $\langle \log_{10} I_\nu \rangle$, and logarithm standard deviation, $\left\langle (\log_{10} I_\nu - \langle \log_{10} I_\nu \rangle)^2 \right\rangle$, a good approximation of the whole distribution. The means and standard deviations for all of the log-background posterior chains can be found in [Figure 3](#), with the blue bar highlighting the official result for this paper, $I_\nu(\lambda = 3.4 \mu\text{m}) = 9.03_{-0.43}^{+0.46} \text{ kJy sr}^{-1}$ ($\nu I_\nu = 7.96_{-0.38}^{+0.40} \text{ nW m}^{-2} \text{ sr}^{-1} e\text{-fold}^{-1}$). The full details of what defines all of the samples that fix the model parameters can be found in [Lake et al. \(2018\)](#). The survey specific samples (above the dotted line) are sorted in order of increasing depth (defined as median redshift) with shallowest on top. The combined samples (below the dotted line) are Low z when the data is limited to redshift $z \leq 0.2$, High z when $0.2 < z \leq 1.0$, Prior when the faint end slope (α) of the LF is constrained using

Table 1. Example Lines from MCMC Background Chains

StepNum	WalkerNum	Inu.1	Inu.5
—	—	kJy sr ⁻¹	kJy sr ⁻¹
0	0	4.6784	9.8475
0	1	4.6598	9.3267
0	2	4.4538	8.7004
0	3	4.5978	9.2741
0	4	4.5714	9.1531

NOTE—Example lines from one of the chains produced by `emcee` in the tables under [DOI 10.6084/m9.figshare.4245443](https://doi.org/10.6084/m9.figshare.4245443). Floating point values truncated here for brevity, but not in the downloadable tables. `StepNum` is the zero indexed step number that the ensemble was at in the chain, and `WalkerNum` is the number of the walker which was at the position defined by the row for that step. `Inu.1` is the contribution of galaxies to the EBL at 3.4 μm for the corresponding element of the chain from [Lake et al. \(2018\)](#) for galaxies at redshift $z < 1$. `Inu.5` is the same but for galaxies with redshift $z < 5$.

the mean and standard deviation of the faint end slope of the corresponding Low z sample, and Trim when the contributions of each survey are limited to areas in the luminosity-redshift plane where the survey is more than 98% of its maximum completeness. In sum, the Trim samples sacrifice sample size and depth for reduced systematic uncertainty, and the Prior samples combine the aspect of the Low z samples least affected by a bias of uncertain origin that affects bright sources.

The important features to note in [Figure 3](#) are: the samples most affected by the unknown bias identified in [Lake et al. \(2018\)](#) (6dFGS, SDSS, Low z , and Low z Trim) have the expected backgrounds so high they can accurately be described as outliers, and there is an increasing trend in the predicted background with survey depth (GAMA, AGES, *WISE*/DEIMOS, and zCOSMOS, in order). The presence of the High z Trim sample in the category of outliers is a consequence of that chain having a mean faint end slope of $\alpha = -1.93 \pm -0.04$, nearer the point where the LF estimate diverges at $\alpha = -2$ than the other samples which all have α nearer to -1 . It is likely that the same fluctuation that makes the α of the High z Trim sample so negative was displaced into a faster comoving number density evolution; one that implies galaxies are presently increasing in comoving number density at $1.9 \pm 0.7 e\text{-folds}$ per Hubble time, reducing the estimated background. For all of these reasons, and because it has the greatest statistical precision, the High z Prior is most likely to prove most accurate when compared with even better, deeper, measurements made in the future.

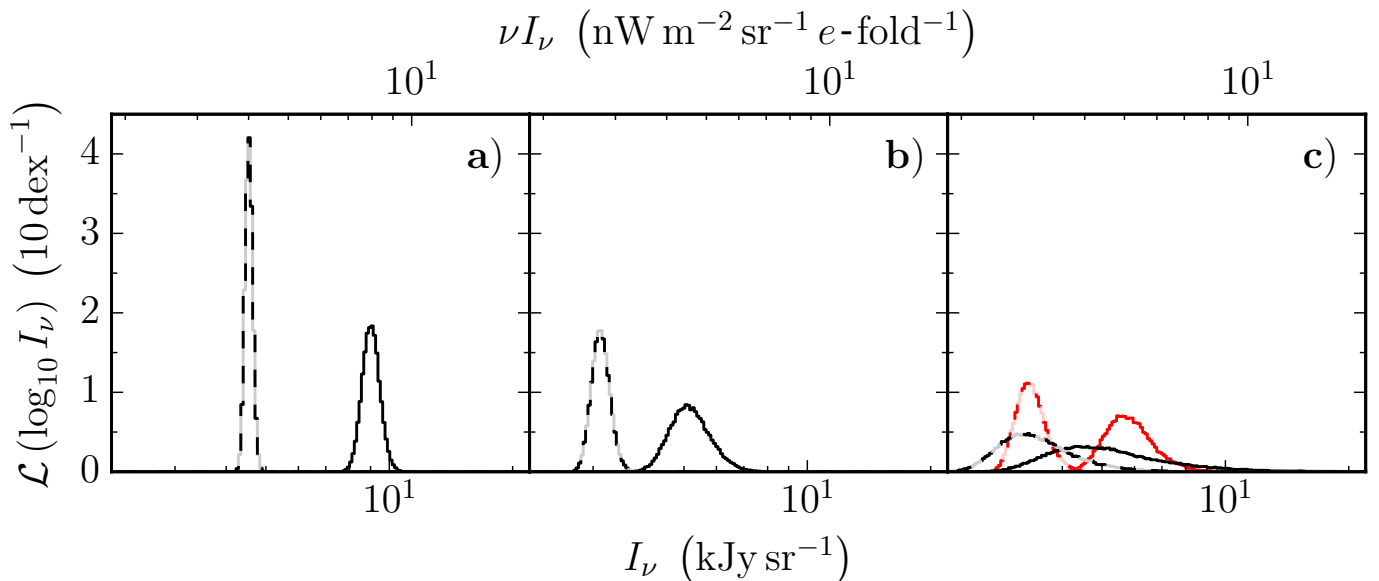


Figure 2. Example EBL Histograms

Histograms of EBL posteriors that correspond to different LF posteriors from Lake et al. (2018). The dashed lines are histograms of the $z \leq 1$ predictions and the solid lines are of the $z \leq 5$. Panel **a** is based on the High z Prior chain, Panel **b** is based on the High z Trim Prior chain, and Panel **c** uses the survey specific chains from *WISE*/DEIMOS (black) and zCOSMOS (red). Each posterior chain contains a total of 210,000 samples.

The priors imposed on the LF parameters in Lake et al. (2018) were chosen to be analytically calculable and minimally informative, with the exception of the parameter that defines the poorly constrained early time behavior of L_* , n_0 . Just as MCMC permits drawing a set of samples from the posterior distribution, it is also possible to sample the prior. This is not usually done, because priors are usually analytically calculable. In this case, though, the prior on the EBL values is not analytically calculable from the prior on the LF parameters (primarily due to the numerical definition of the mean galaxy SED). The EBL prior must, therefore, be reconstructed from Monte Carlo samples drawn from the LF prior. Because the EBL prior is entirely determined by priors set on other parameters, it is described here as being ‘induced’ implicitly by the prior on the LF parameters. A portion of a histogram of the induced EBL prior chain can be found in Figure 4 (the range was restricted to what is relevant for the posterior chains in this work). Some example lines from the EBL prior chain file can be found in Table 2. The black line is the histogram of the $z \leq 5$ background, and the grey line is of the $z \leq 1$ background, offset to the right by 26 millidex, for clarity. The prior is clearly not flat in either I_ν or $\ln I_\nu$ in the region of interest. It is, in fact, slightly biased to the low side. Note that the response of a log-normal distribution, $f(\ln(x)) \propto \exp(-[\ln x - \mu]^2/[2\sigma^2])$, to a prior that is approximable as x^k (here $k \approx -0.5$ for most of the range of interest) is to shift it by an

amount that depends on the width of the distribution, $\delta\mu = k\sigma^2$. Because $|k\sigma| < 1$ for all of the posteriors produced here, the shift will be less than σ in all cases; for the High z Prior result, in particular, the shift in the mean caused by the prior is the same as dividing the mean I_ν by 0.998. The backgrounds that correspond to the induced EBL prior MCMC chain are published alongside this article as a machine readable table, and under DOI:10.6084/m9.figshare.8142284.

The evolving spectral luminosity density and EBL are plotted in Figure 5. The evolution in the luminosity density, depicted in panels **a** and **c**, arises entirely from normalization (evolution of luminosity function parameters) and redshifting of the mean SED. The evolving EBL, depicted in panels **b** and **d**, loses the spectral features visible in the luminosity density, as the integration smears them out and expansion redshifts old photons away. Most other works depict the optical region of the EBL peaking between 1 and 2 μm (see, for example, Domínguez et al. (2011) and Cooray (2016)), but that is the result of plotting νI_ν , where Figure 5 plots I_ν . The data used to produce the plots are included with this work as fits tables, and under 10.6084/m9.figshare.4757131.

5. DISCUSSION

The models used to calculate the 3.4 μm EBL in this work have two shortcomings most relevant to the EBL estimate. First, the mean SED did not evolve with lumi-

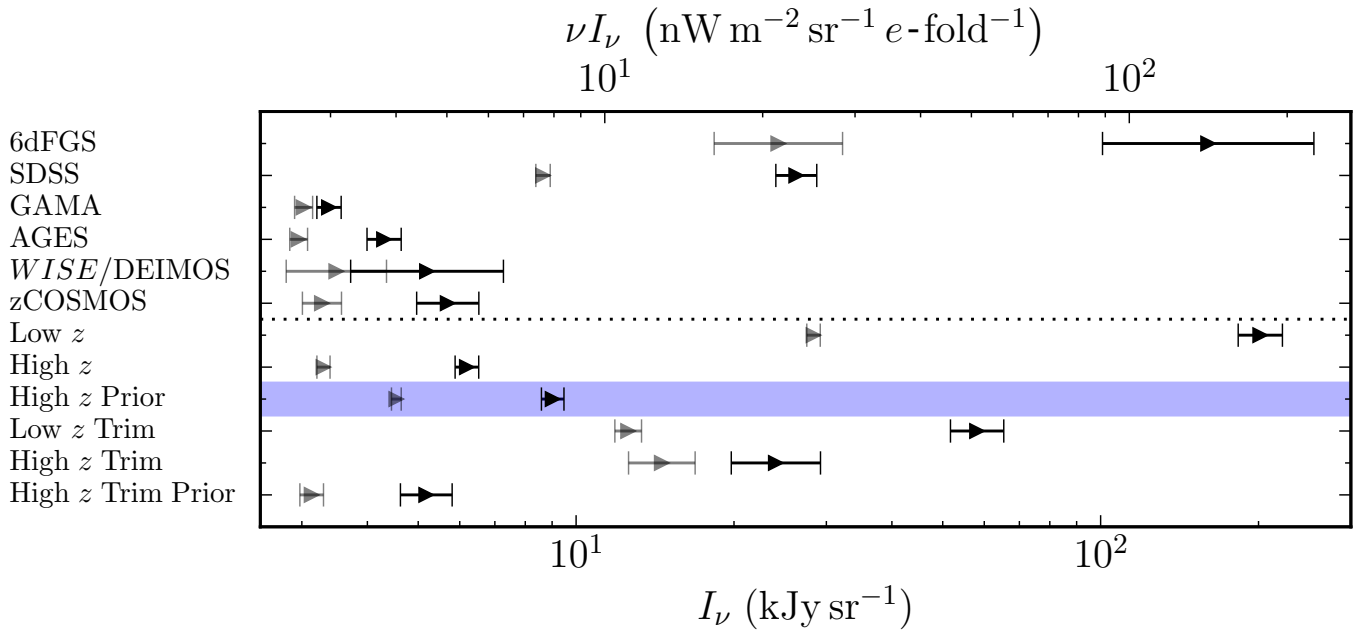


Figure 3. EBL and Uncertainties for Different Chains

All of the 3.4 μm EBL predictions made using the posterior chains from Lake et al. (2018). The grey points are the $z \leq 1$ backgrounds, and the black points are the $z \leq 5$ ones. The dotted lines divides the survey based samples (above) from the combined samples (below). The blue bar highlights background based on the canonical chain from Lake et al. (2018).

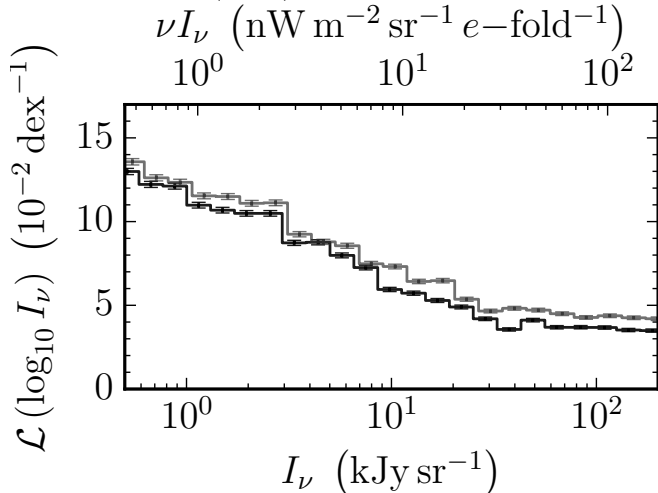


Figure 4. Induced Prior on the EBL Estimates

The relevant part of the EBL prior induced by the priors on the LF parameters in Lake et al. (2018). The black line is the prior for $z \leq 5$ backgrounds, and the grey line is for the $z \leq 1$ backgrounds. The grey line is shifted to the right by 26 milli-dex. The chain used to construct this histogram contained 322,560 samples, in total, spanning more than 30 orders of magnitude (the priors on the LF parameters were very broad), and the error bars are approximated by assuming Poisson statistics. Note that the black and grey lines are not independent, since they were calculated using the same MCMC LF parameter chains.

Table 2. Example Lines from MCMC Induced Prior Background Chains

Inu.1	Inu.5
kJy sr $^{-1}$	kJy sr $^{-1}$
2.0879	2.0879
0.5818	0.5818
0.5818	0.5818
0.5818	0.5818
0.5818	0.5818

NOTE—Example lines from the induced background posterior chain produced by `emcee` in the table under DOI [10.6084/m9.figshare.8142284](https://doi.org/10.6084/m9.figshare.8142284). Floating point values truncated here for brevity, but not in the downloadable tables. Inu.1 is the contribution of galaxies to the EBL at 3.4 μm for galaxies at redshift $z < 1$, and Inu.5 is the same but for galaxies with redshift $z < 5$.

osity or redshift. Second, the faint end slope of the LF was also a constant. Figure 6 contains a plot highlight-

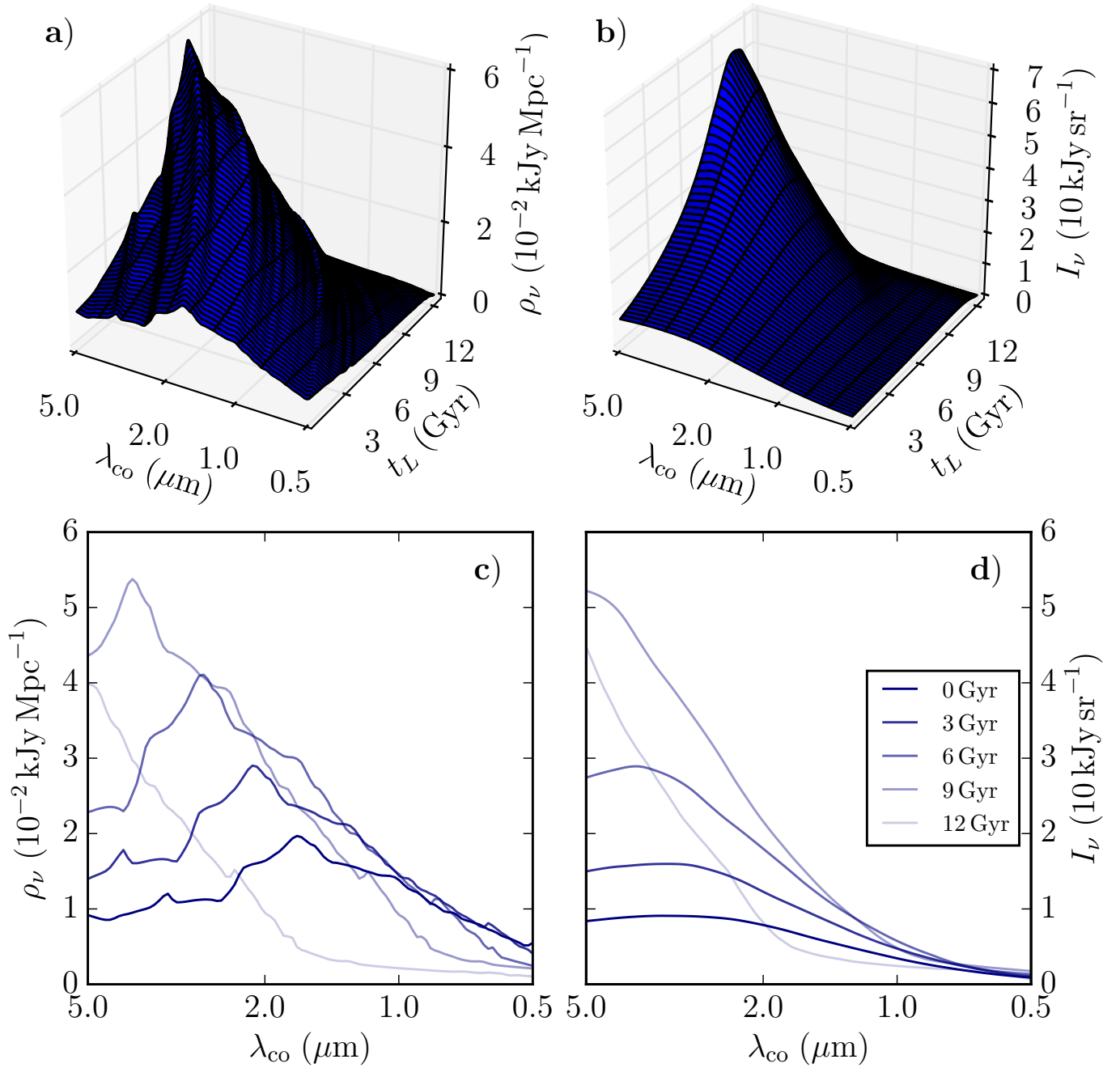


Figure 5. Evolving Luminosity Density and Background

Panels **a** and **b** are 3-dimensional plots of the comoving spectral luminosity density (see Equation 2) and the EBL (I_ν) as a function of comoving/coordinate wavelength (λ_{co}) and lookback time ($t_L(z)$). The redshifts spanned are from 0 to 5. Panels **c** and **d** are constant time slices from the above panels (at 0 through 12 Gyr in steps of 3 Gyr), with decreasing opacity (darkness) as t_L increases. Note how the EBL roughly tracks the luminosity density at the given epoch, though the detailed spectral features are smeared out.

ing where in redshift-luminosity space the 3.4 μm EBL originates. As expected, the model predicts that the EBL is dominated by low to moderate redshift objects with luminosities near L_* . Studies of the high redshift universe consistently show that galaxies in the early universe have optical and ultraviolet spectra dominated by high mass stars, making them, on average, more blue than low redshift galaxies. Bouwens et al. (2009) and Bouwens et al. (2014), for example, found that galaxies exhibited a trend of bluer ultraviolet slope, decreasing $\beta = \frac{d \ln L_\lambda}{d \ln \lambda}$, for both increasing redshift and decreasing luminosity. Similarly, studies of the mass function of galaxies show a trend of decreasing α with increasing redshift (see the compilation in Table 1 of Conselice et al. 2016) to a minimum around the -2 predicted by the ΛCDM models in Jenkins et al. (2001).

Both color evolution and faint end slope evolution suggest that the EBL measurements produced here are underestimates. The former would tend to increase size of the high redshift tail of the bottom plot in Figure 6, and the latter would increase the low luminosity tail of the left hand plot in the same figure. These factors are counter-balanced by the fact that the model has slower evolution in L_* at high redshift than would be suggested by comparisons with Figure 9 of Madau & Dickinson (2014), which would narrow the high redshift tail.

It is difficult to predict how these competing factors will work out when more accurate measurements are available. The SED evolution is unlikely to contribute more than a factor of 10 to the thickness of the high redshift tail. Evolution in L_* is likely to be of a similar size. The interesting challenge is presented by the evolution in α , where measurements with $\alpha \leq -2$ require the explicit addition of a low luminosity cutoff to the LF to produce a finite contribution to the background. This means that fully constraining the contribution of galaxies to the EBL will require measuring galaxies on the faint end slope of the LF to either eliminate $\alpha \leq -2$ or to find the LF's faint end cutoff. Interestingly, the presence of a faint end cutoff, L_{min} , with a steep faint end slope, $\alpha \leq -2$, increases the impact that L_* evolution has on the predicted EBL because L_{min} enters into EBL calculations in a ratio with L_* .

Figure 7 shows how the primary estimate in this work compares with values from the literature from wavelengths in the range 3.4 to 3.6 μm , adjusted to 3.4 μm assuming I_ν is approximately a constant with wavelength. Points in Figure 7 include direct observations of the EBL (Sano et al. 2016; Tsumura et al. 2013; Levenson et al. 2007; Matsumoto et al. 2005; Wright & Johnson 2001; Wright & Reese 2000; Gorjian et al. 2000), upper limits based on the examination of the extinction

of TeV gamma rays from blazar spectra (Mazin & Raue 2007; Aharonian et al. 2006), estimates of the contribution of galaxies based on extrapolating galaxy source flux counts (Driver et al. 2016; Levenson & Wright 2008; Fazio et al. 2004), and other LF based estimates (Stecker et al. 2016; Helgason et al. 2012; Domínguez et al. 2011). What can be seen from the comparisons is that, while the 3.4 μm EBL measured here is higher than measurements from most comparable works, it is still consistent **with** the blazar limits and the direct measurements. Judging by the relationship to the literature measurements, any modification from the true value caused by the systematic limitations in this work is unlikely be more than about 2 kJy sr^{-1} (1.8 nW m^{-2} sr^{-1} e-fold) in either direction.

Further confirmation of the basic accuracy of the model used to predict the EBL can be found from comparing observed source flux counts to predicted ones across different wavelengths. Figures 8 and 9 contain comparisons of the observed source flux histograms (black lines) to the predicted contribution of galaxies based on the mean LF of the posterior chains produced from the High z Prior, High z Trim Prior, and *WISE*/*DEIMOS* samples (red, blue, and grey dashed lines, respectively), and a simple power law model fit to a subset of the data in each plot (orange dash-dotted line) that is, nominally ‘stars’ (the subset range is highlighted in orange in the plots under the main one in the panel). The fit parameters are not reported here because they are beyond the scope of this work. The top rows contain direct comparisons with multiple models, and the bottom rows show the fractional residual counts with Poisson uncertainties after subtracting off the sum of the stars model and the High z Prior model (model counts in the denominator).

Figure 8 contains comparisons to the AllWISE flux counts for all sources within the northern galactic cap ($b \geq 30^\circ$) that have no artifact flags set and a signal to noise ratio (SNR) at least 4 in the plotted band, giving a total of 650, 47, and 4.7 million sources in panels **a–c**, respectively. The plotted flux is the standard point spread function (psf) flux, so it will have inaccuracies at the bright end. Those inaccuracies are unobservable, though, because no effort was made to separate stars from galaxies and the star counts dominate there. No completeness corrections were applied to any of the data, either, so the faint end of the observations is expected to undershoot the predictions.

Figure 9 contains counts from the Sloan Digital Sky Survey (SDSS) data release 10 database table named *PhotoObj*. The information in the plots shown in Figure 9 is nearly identical to the ones

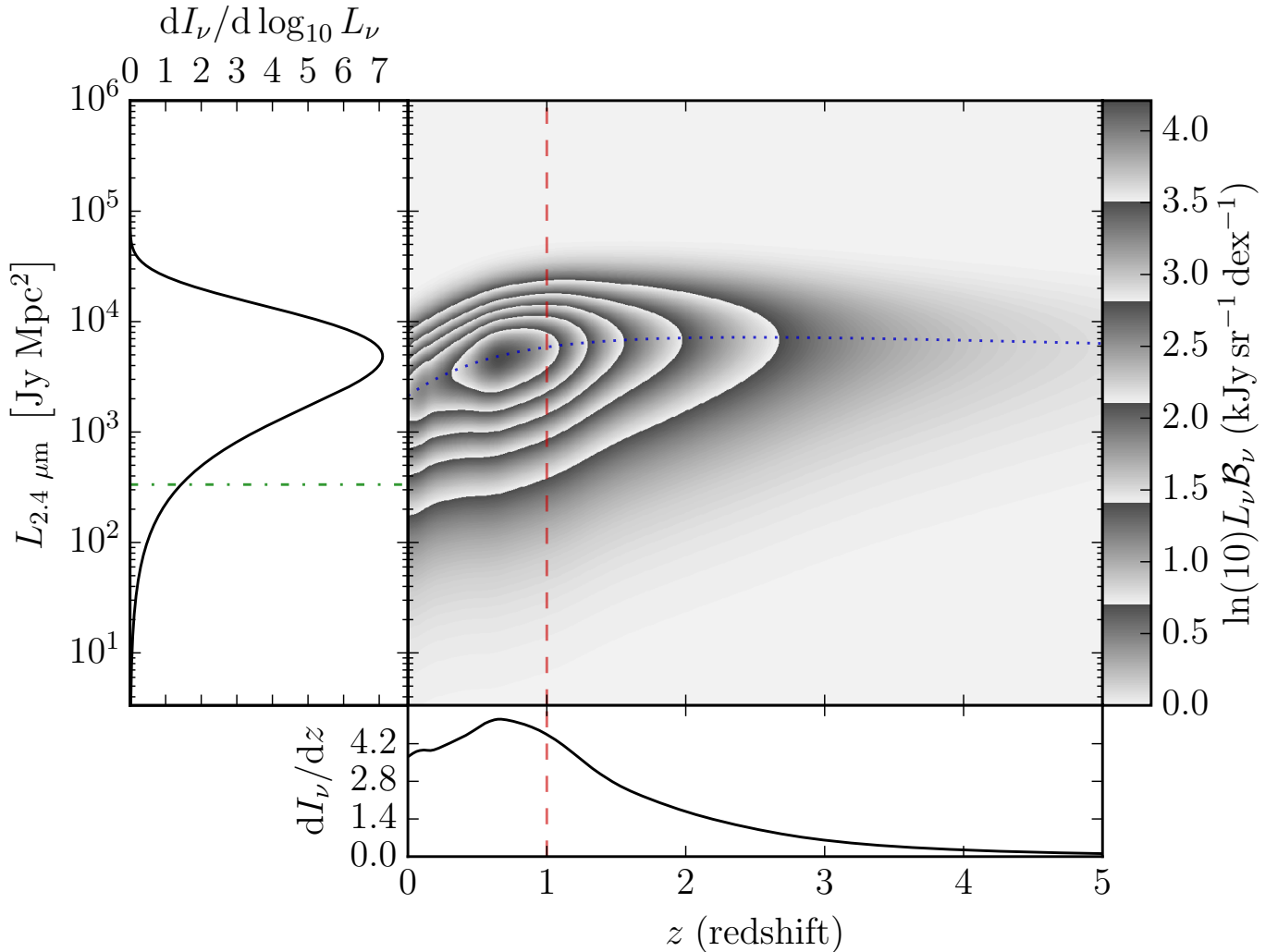


Figure 6. Density of Contributions to the EBL by Redshift and Luminosity

Bivariate density of contributions to the $3.4 \mu\text{m}$ EBL by galaxies according to the mean model from the High z Prior MCMC posterior chain, with the marginal densities abutting. The blue dotted line on the bivariate density shows the evolution of L_* , the red vertical dashed line highlights the extent of the data the models were fit to, and the green dash-dotted line marks $10^{10} L_{2.4 \mu\text{m} \odot}$ (where the galaxy’s spectral luminosity, L_ν , at wavelength $\lambda = 2.4 \mu\text{m}$ is the same as L_ν at the same point in the spectrum as 10^{10} suns). The total $3.4 \mu\text{m}$ background in this plot is 9.06 kJy sr^{-1} ($7.99 \text{ nW m}^{-2} \text{ sr}^{-1} e\text{-fold}$).

from Figure 8, with the one major change being that the extinction correction in the SDSS columns `extinction_[band letter]` were applied. The SDSS sources are limited to two circular regions with 9° radius that are nearly antipodes – centered at J2000 right ascension and declination ($163.56309^\circ, 7.27216^\circ$) and ($343.56309^\circ, -1.27216^\circ$). A source is excluded if it has any of the following flags, as explained in the SDSS database schema browser⁵, set for the band in question (column named `flags_[band letter]`): `EDGE`, `BLENDED`, `NODEBLEND`, `SATURATED`, `TOO_LARGE`, `MOVED`, `MAYBE_CR`,

and `MAYBE_EGHOST`. Each source also had to have an $\text{SNR} \geq 4$, just like the AllWISE sources, giving a total of 6.4, 8.5, 9.0, 1.5, and 4.9 million sources in panels **a–e**, respectively. The plotted fluxes are the `modelFlux_[band letter]` columns, so they won’t describe stars accurately, but that shouldn’t matter for the same reason the psf fluxes do not meaningfully affect the AllWISE plots.

What the plots in Figures 8 and 9 show is that the model used here performs better than expected in predicting the number counts at wavelengths where the Gaussian approximation of \mathcal{L}_{SED} is no longer valid (particularly SDSS g and u). In all wavelengths and for all of the predictions plotted, the flux counts predictions are

⁵ <http://skyserver.sdss.org/dr10/en/help/browser/browser.aspx#&&history=enum+PhotoFlags+E>

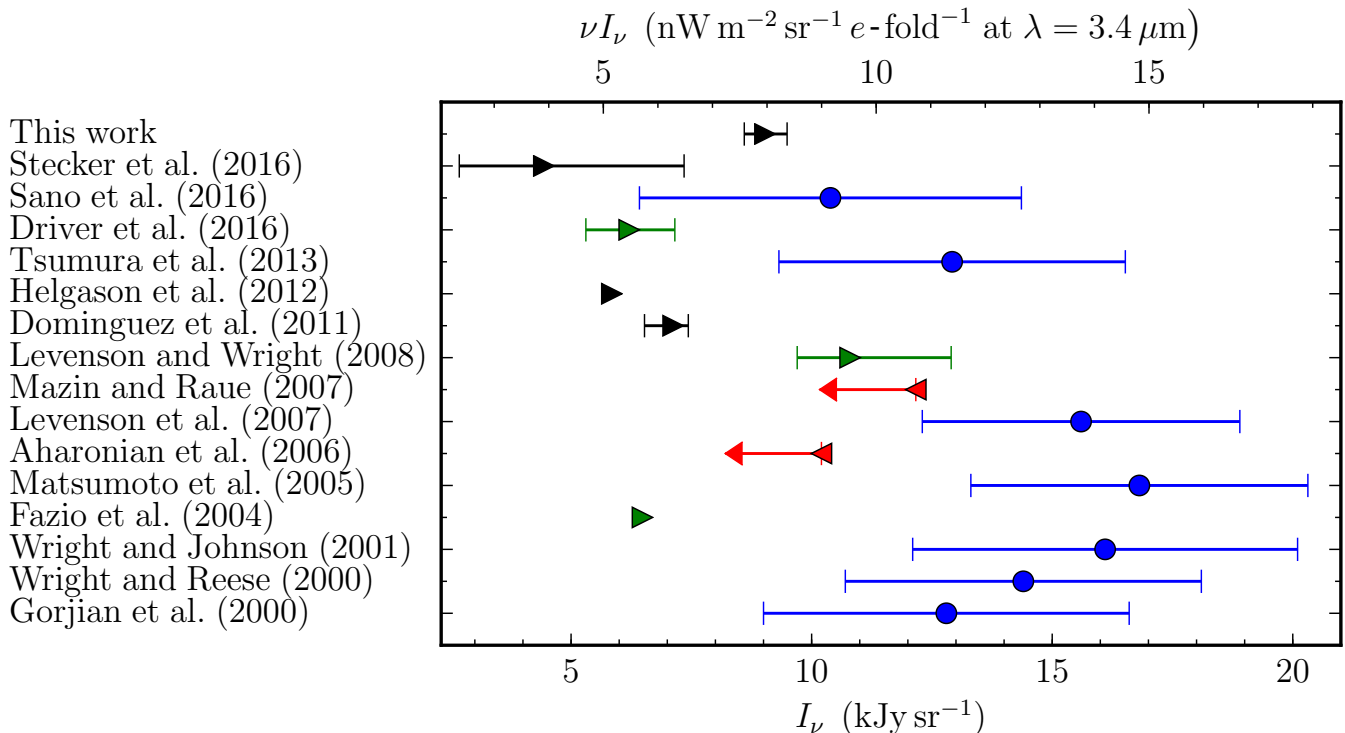


Figure 7. 3.4 μm EBL Measurements

Comparison of different values measured for the EBL for wavelengths near 3.4 μm ordered by year of publication then first author last name. The points plotted as blue circles are direct observations of the EBL, the green triangles are based on integrating extrapolated galaxy flux histograms to 0, the red inverted triangles are upper limits from blazar extinction models, and the black triangles are luminosity function based estimates of what galaxies contribute to the EBL. Points without error bars (Fazio et al. 2004; Helgason et al. 2012) did not include error estimates in the original work.

reasonably close to the observed histograms. The comparison makes clear how, using flux counts alone or using LFs measured at different wavelengths, it would be easy to get an estimate of the 3.4 μm background to be closer to the 5 ± 1 kJy sr^{-1} of the High z Trim Prior based estimates, plotted in blue, than the High z Prior based estimate, plotted in red, depending on how strict the definition of ‘galaxy’ is and how incompleteness at the faint end is modeled. The comparisons also show that there is still untapped information that can be used to more tightly constrain the full spectro-luminosity functional in future works. The over-prediction at the faint end of the W1 plot is to be expected because of incompleteness from both the limit of photometric sensitivity⁶ and confusion⁷, though the level of over-prediction for the High- z Prior model at the faint end means it should be viewed as suspect for the purposes of predicting faint galaxy flux counts.

⁶ http://wise2.ipac.caltech.edu/docs/release/allwise/expsup/sec2_4a.html

⁷ http://wise2.ipac.caltech.edu/docs/release/allsky/expsup/sec6_2.html#brt_stars

6. CONCLUSION

We showed from analyzing the mean SED of galaxies using more than a thousand galaxies with an average of more than 5 photometric observations of each galaxy, and the 2.4 μm LF of galaxies using more than half a million galaxies with spectroscopic redshifts, that the contribution of galaxies to EBL at 3.4 μm is $I_\nu = 9.0 \pm 0.5$ kJy sr^{-1} ($\nu I_\nu = 8.0 \pm 0.4$ $\text{nW m}^{-2} \text{sr}^{-1} e\text{-fold}$), with systematic uncertainties unlikely to be greater than 2 kJy sr^{-1} . This value is consistent with both direct measures of the background and constraints based on blazar spectra. Recent work on the production of gamma rays by blazar protons relaxes the strength of these constraints (Essey & Kusenko 2010; Essey et al. 2011; Aharonian et al. 2013), leaving room for contributions from extended galaxy halos (discussed in Cooray et al. 2012) and from a large faint galaxy population implied by the steepening faint end slope of the mass function (compiled in Conselice et al. 2016). Settling the contribution from high z faint galaxies will require deeper redshift surveys, to more firmly establish the steepness of the faint end slope, and work to establish how the faint end of the LF cuts off. Two examples

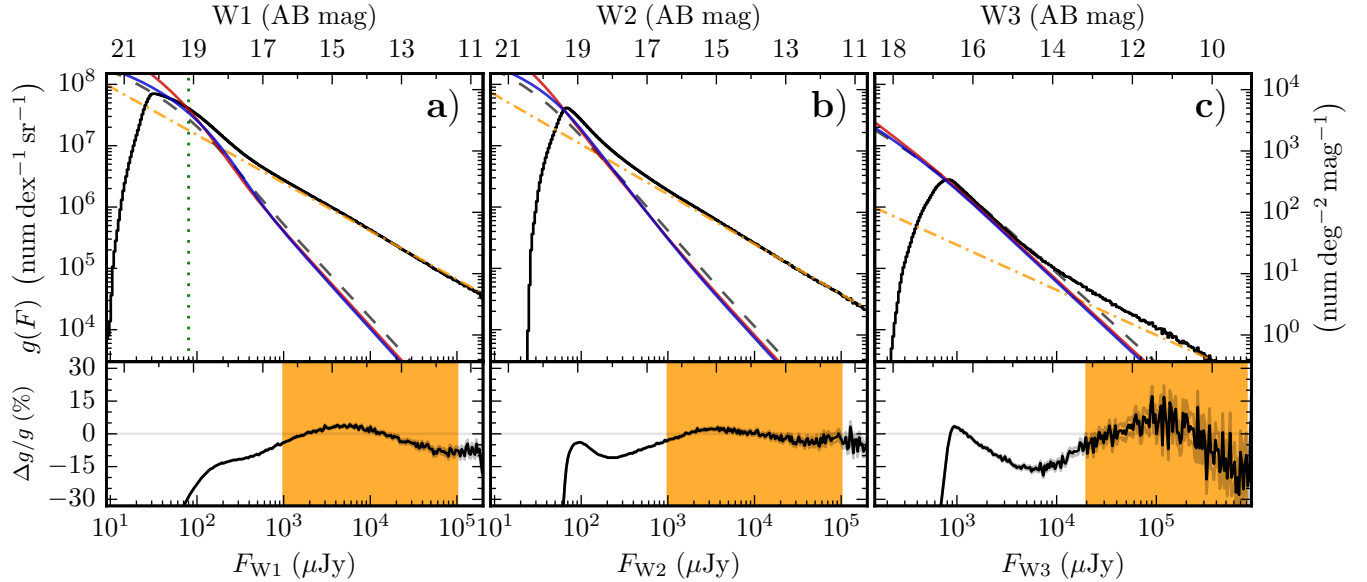


Figure 8. WISE Flux Counts Comparisons

Comparisons of the predicted source flux counts, $g(f) \equiv \frac{d^2 N}{d \log_{10} F d \Omega}$ from the MCMC chain mean $g(f)$ models of Lake et al. (2018), to observed flux counts (solid black line) in the AllWISE W1, W2, and W3 bands in the top panels. The bottom panels show the residuals of the data with respect to the High z Prior model added to a power law ‘star’ model. The three galaxy predictions plotted are based on the mean LFs from the samples Lake et al. (2018) labeled as High z Prior (red line), High z Trim Prior (blue line), and WISE/DEIMOS (grey dashed line). A power law model (orange dash-dotted line) was added to the High z Prior model and fit to the data in the region highlighted in orange in each plot’s lower panel.

of possible mechanisms that can provide a faint end cutoff to the LF are: an intrinsic lower bound to the halo mass function, and a deviation in the halo mass to light conversion factor (caused, for example, by a lower limit on the halo mass capable of accreting and cooling baryons from the inter-galactic medium into star forming clouds).

7. ACKNOWLEDGEMENTS

We would like to thank the anonymous reviewer for the helpful suggestions that improved the quality of this work.

This publication makes use of data products from the Wide-field Infrared Survey Explorer, which is a joint project of the University of California, Los Angeles, and the Jet Propulsion Laboratory/California Institute of Technology, and NEOWISE, which is a project of the Jet Propulsion Laboratory/California Institute of Technology. WISE and NEOWISE are funded by the National Aeronautics and Space Administration.

Funding for SDSS-III has been provided by the Alfred P. Sloan Foundation, the Participating Institutions, the National Science Foundation, and the U.S. Department of Energy Office of Science. The SDSS-III web site is <http://www.sdss3.org/>.

SDSS-III is managed by the Astrophysical Research Consortium for the Participating Institutions of the

SDSS-III Collaboration including the University of Arizona, the Brazilian Participation Group, Brookhaven National Laboratory, Carnegie Mellon University, University of Florida, the French Participation Group, the German Participation Group, Harvard University, the Instituto de Astrofísica de Canarias, the Michigan State/Notre Dame/JINA Participation Group, Johns Hopkins University, Lawrence Berkeley National Laboratory, Max Planck Institute for Astrophysics, Max Planck Institute for Extraterrestrial Physics, New Mexico State University, New York University, Ohio State University, Pennsylvania State University, University of Portsmouth, Princeton University, the Spanish Participation Group, University of Tokyo, University of Utah, Vanderbilt University, University of Virginia, University of Washington, and Yale University.

This research has made use of the NASA/ IPAC Infrared Science Archive, which is operated by the Jet Propulsion Laboratory, California Institute of Technology, under contract with the National Aeronautics and Space Administration.

RJA was supported by FONDECYT grant number 1191124.

Funded by Chinese Academy of Sciences Presidents International Fellowship Initiative. Grant No. 2019PM0017.

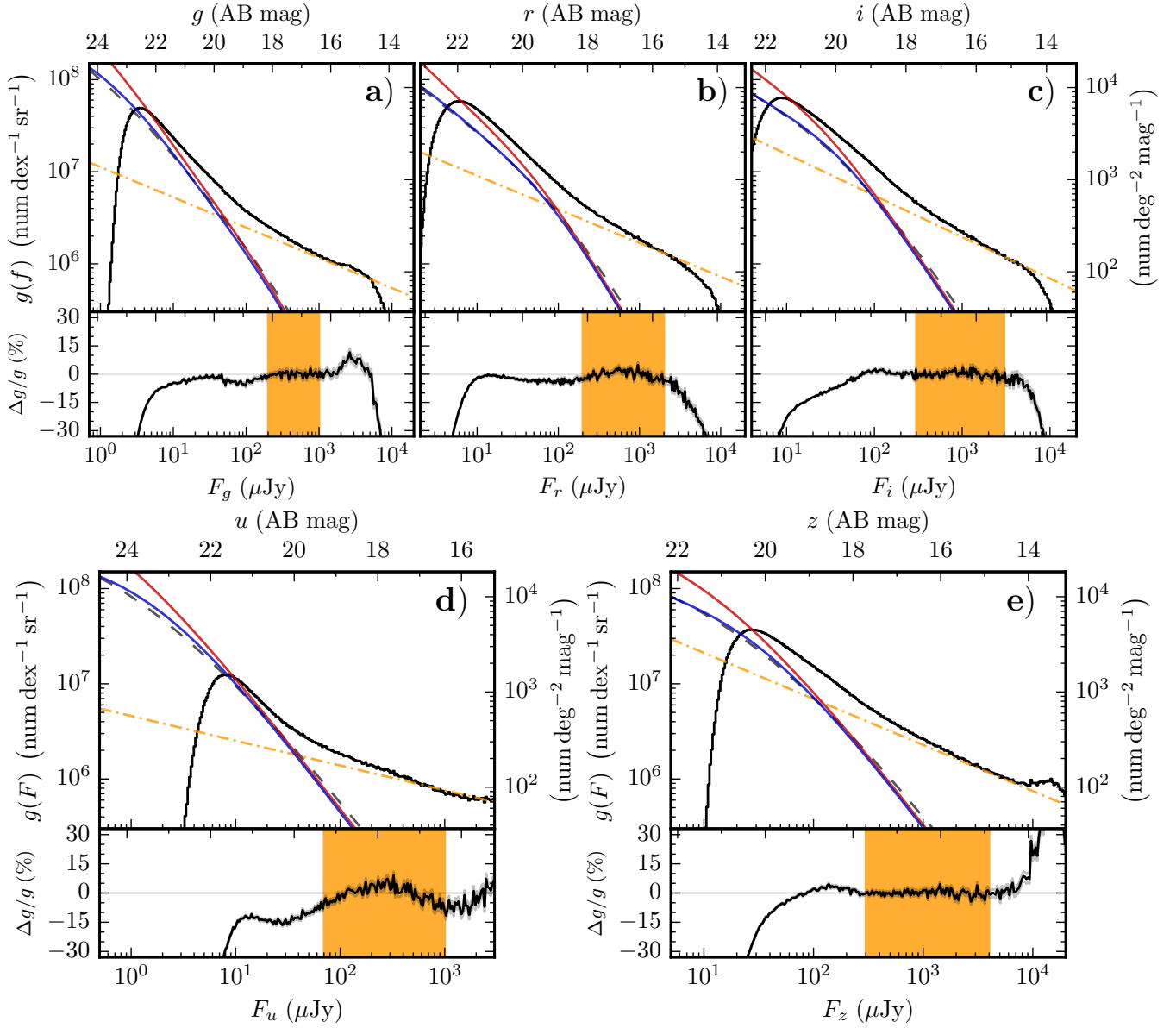


Figure 9. SDSS Flux Counts Comparisons

The same comparison as shown in Figure 8, but to a sample of SDSS selected sources in g , r , i , u , and z bands for panels a–e, respectively.

This project is partially supported by the CAS International Partnership Program

No.114A11KYSB20160008 and CAS Interdisciplinary Innovation Team.

REFERENCES

- Aharonian, F., Essey, W., Kusenko, A., & Prosekin, A. 2013, *PhRvD*, 87, 063002, doi: [10.1103/PhysRevD.87.063002](https://doi.org/10.1103/PhysRevD.87.063002)
- Aharonian, F., Akhperjanian, A. G., Bazer-Bachi, A. R., et al. 2006, *Nature*, 440, 1018, doi: [10.1038/nature04680](https://doi.org/10.1038/nature04680)
- Assef, R. J., Kochanek, C. S., Brodwin, M., et al. 2010, *ApJ*, 713, 970, doi: [10.1088/0004-637X/713/2/970](https://doi.org/10.1088/0004-637X/713/2/970)
- Bouwens, R. J., Illingworth, G. D., Franx, M., et al. 2009, *ApJ*, 705, 936, doi: [10.1088/0004-637X/705/1/936](https://doi.org/10.1088/0004-637X/705/1/936)
- Bouwens, R. J., Illingworth, G. D., Oesch, P. A., et al. 2014, *ApJ*, 793, 115, doi: [10.1088/0004-637X/793/2/115](https://doi.org/10.1088/0004-637X/793/2/115)

- Cambr esy, L., Reach, W. T., Beichman, C. A., & Jarrett, T. H. 2001, *ApJ*, 555, 563, doi: [10.1086/321470](https://doi.org/10.1086/321470)
- Conselice, C. J., Wilkinson, A., Duncan, K., & Mortlock, A. 2016, *ApJ*, 830, 83, doi: [10.3847/0004-637X/830/2/83](https://doi.org/10.3847/0004-637X/830/2/83)
- Cooray, A. 2016, *Royal Society Open Science*, 3, 150555, doi: [10.1098/rsos.150555](https://doi.org/10.1098/rsos.150555)
- Cooray, A., Smidt, J., De Bernardis, F., et al. 2012, *Nature*, 490, 514. <http://dx.doi.org/10.1038/nature11474>
- Dom nguez, A., Primack, J. R., Rosario, D. J., et al. 2011, *MNRAS*, 410, 2556, doi: [10.1111/j.1365-2966.2010.17631.x](https://doi.org/10.1111/j.1365-2966.2010.17631.x)
- Driver, S. P., Andrews, S. K., Davies, L. J., et al. 2016, *ApJ*, 827, 108, doi: [10.3847/0004-637X/827/2/108](https://doi.org/10.3847/0004-637X/827/2/108)
- Essey, W., Kalashev, O., Kusenko, A., & Beacom, J. F. 2011, *ApJ*, 731, 51, doi: [10.1088/0004-637X/731/1/51](https://doi.org/10.1088/0004-637X/731/1/51)
- Essey, W., & Kusenko, A. 2010, *Astroparticle Physics*, 33, 81, doi: [10.1016/j.astropartphys.2009.11.007](https://doi.org/10.1016/j.astropartphys.2009.11.007)
- Fazio, G. G., Ashby, M. L. N., Barmby, P., et al. 2004, *ApJS*, 154, 39, doi: [10.1086/422585](https://doi.org/10.1086/422585)
- Gorjian, V., Wright, E. L., & Chary, R. R. 2000, *ApJ*, 536, 550, doi: [10.1086/308974](https://doi.org/10.1086/308974)
- Helgason, K., Ricotti, M., & Kashlinsky, A. 2012, *ApJ*, 752, 113, doi: [10.1088/0004-637X/752/2/113](https://doi.org/10.1088/0004-637X/752/2/113)
- Hinshaw, G., Larson, D., Komatsu, E., et al. 2013, *ApJS*, 208, 19, doi: [10.1088/0067-0049/208/2/19](https://doi.org/10.1088/0067-0049/208/2/19)
- Jenkins, A., Frenk, C. S., White, S. D. M., et al. 2001, *MNRAS*, 321, 372, doi: [10.1046/j.1365-8711.2001.04029.x](https://doi.org/10.1046/j.1365-8711.2001.04029.x)
- Knobel, C., Lilly, S. J., Iovino, A., et al. 2012, *ApJ*, 753, 121, doi: [10.1088/0004-637X/753/2/121](https://doi.org/10.1088/0004-637X/753/2/121)
- Lake, S. E., & Wright, E. L. 2016, *The Open Journal of Astrophysics*, doi: [10.21105/astro.1603.07299](https://doi.org/10.21105/astro.1603.07299)
- Lake, S. E., Wright, E. L., Assef, R. J., et al. 2018, *ApJ*, 866, 45, doi: [10.3847/1538-4357/aadd47](https://doi.org/10.3847/1538-4357/aadd47)
- Lake, S. E., Wright, E. L., Tsai, C.-W., & Lam, A. 2017, *AJ*, 153, 189, doi: [10.3847/1538-3881/aa643a](https://doi.org/10.3847/1538-3881/aa643a)
- Levenson, L. R., & Wright, E. L. 2008, *ApJ*, 683, 585, doi: [10.1086/589808](https://doi.org/10.1086/589808)
- Levenson, L. R., Wright, E. L., & Johnson, B. D. 2007, *ApJ*, 666, 34, doi: [10.1086/520112](https://doi.org/10.1086/520112)
- Lilly, S. J., Le Brun, V., Maier, C., et al. 2009, *ApJS*, 184, 218, doi: [10.1088/0067-0049/184/2/218](https://doi.org/10.1088/0067-0049/184/2/218)
- Lin, H., Yee, H. K. C., Carlberg, R. G., et al. 1999, *ApJ*, 518, 533, doi: [10.1086/307297](https://doi.org/10.1086/307297)
- Madau, P., & Dickinson, M. 2014, *ARA&A*, 52, 415, doi: [10.1146/annurev-astro-081811-125615](https://doi.org/10.1146/annurev-astro-081811-125615)
- Matsumoto, T., Matsuura, S., Murakami, H., et al. 2005, *ApJ*, 626, 31, doi: [10.1086/429383](https://doi.org/10.1086/429383)
- Mazin, D., & Raue, M. 2007, *A&A*, 471, 439, doi: [10.1051/0004-6361:20077158](https://doi.org/10.1051/0004-6361:20077158)
- Sano, K., Kawara, K., Matsuura, S., et al. 2016, *ApJ*, 818, 72, doi: [10.3847/0004-637X/818/1/72](https://doi.org/10.3847/0004-637X/818/1/72)
- Stecker, F. W., Scully, S. T., & Malkan, M. A. 2016, *ApJ*, 827, 6, doi: [10.3847/0004-637X/827/1/6](https://doi.org/10.3847/0004-637X/827/1/6)
- Tsumura, K., Matsumoto, T., Matsuura, S., Sakon, I., & Wada, T. 2013, *PASJ*, 65, doi: [10.1093/pasj/65.6.121](https://doi.org/10.1093/pasj/65.6.121)
- Wright, E. L., & Johnson, B. D. 2001, *ArXiv Astrophysics e-prints*
- Wright, E. L., & Reese, E. D. 2000, *ApJ*, 545, 43, doi: [10.1086/317776](https://doi.org/10.1086/317776)